Mesoporous Silicates with Spherical Morphology Modified with Vanadium Highly Active in Oxidation of Cyclohexene with H2O2

Topics in Catalysis

ISSN 1022-5528
Volume 54
Combined 1-4

Top Catal (2011) 54:160-169
DOI 10.1007/
s11244-011-9635-8

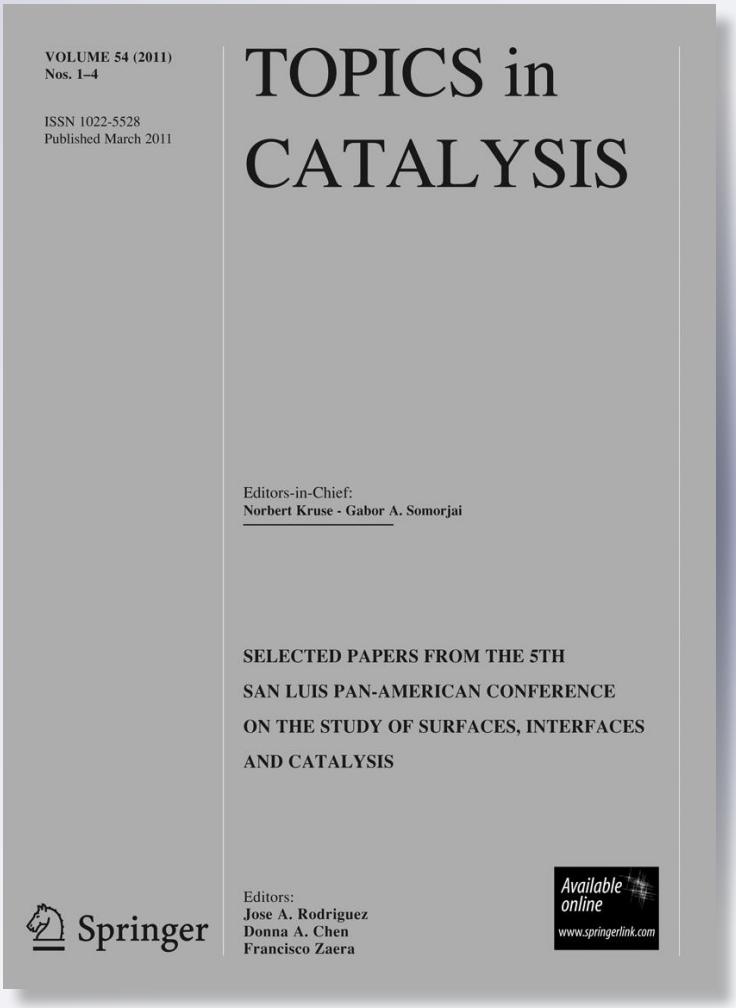

Springer

Top Catal (2011) 54:160–169
DOI 10.1007/s11244-011-9635-8

ORIGINAL PAPER

Mesoporous Silicates with Spherical Morphology Modified with Vanadium Highly Active in Oxidation of Cyclohexene with H_2O_2

Corina M. Chanquía · Analía L. Cánepa · Karim Sapag · Patricio Reyes · Eduardo R. Herrero · Sandra G. Casuscelli · Griselda A. Eimer

Published online: 8 February 2011

Abstract Vanadium-containing mesoporous molecular sieves have been prepared by hydrothermal treatment at 373 K. These materials showed spherical morphology with a narrow particle size distribution between 2 and 4 μm. The techniques used for their physicochemical characterization were: XRD, AAS, N_2 physisorption, SEM, TEM and DR–UV–Vis spectroscopy. All the materials presented high specific surface area (>900 m^2/g), characteristic of MCM-41 materials. A well-defined mesoporous structure was observed by TEM measures although there was no one-dimensional ordering of pores characteristic of such materials. Additionally, secondary mesoporosity domains were determined in the BJH size distribution. The sample synthesized with the highest content of V presented marked differences in their structural characteristics, which were attributed to the blockage of channels by the presence of nano-clusters and/or V_xO_y nano-oxides. From the DR–UV–Vis analysis, a successful incorporation of V ions to silica structure in tetrahedral coordination with oxygen of the network could be inferred. The catalytic activity of these materials was evaluated in the test reaction of cyclohexene oxidation using H_2O_2 as oxidizing agent, showing a high conversion of about 93% respect to the maximum, resulting dominant the radicalary mechanism over the direct oxidation mechanism. Apparently, the isolated V ions incorporated into the silica structure would be responsible for the high catalytic activity of these materials.

Keywords Spheres · Mesoporous silicates · Nano-sized · Vanadium · Isolated species · Cyclohexene · Oxidation · H_2O_2

C. M. Chanquía · A. L. Cánepa · E. R. Herrero · S. G. Casuscelli · G. A. Eimer (✉)
Facultad Regional Córdoba, Centro de Investigación y Tecnología Química (CITeQ), Universidad Tecnológica Nacional, Córdoba 5016, Argentina
e-mail: geimer@scdt.frc.utn.edu.ar

K. Sapag
Laboratorio de Ciencias de Superficies y Medios Porosos (LaCSuMP), Departamento de Física, Instituto de Física Aplicada (INFAP), CONICET, Universidad Nacional de San Luis, San Luis 5700, Argentina

P. Reyes
Facultad de Ciencias Químicas, Universidad de Concepción, Casilla 3-C, Concepción, Chile

C. M. Chanquía · A. L. Cánepa · K. Sapag · S. G. Casuscelli · G. A. Eimer
CONICET, Avenida Rivadavia 1917, C1033AAJ Buenos Aires, Argentina

1 Introduction

Nanotechnology has become a very active and vital area of research, which is rapidly developing in industrial sectors and spreading to almost every field of science and engineering. The literature continually reports new discoveries of unusual phenomena as material structures approach the nanometer scale due to substantial alteration of their fundamental physical and chemical properties. Among these materials, nano-structured silica modified with transition metals, have occupied a central place in heterogeneous catalysis for many years. Nanotechnology has now opened the possibility to control the shape, size and chemical state of these materials. Thus, it is in the synthesis and design of a heterogeneous catalyst, that nanotechnology offers the most significant benefits such as exquisite control over the formation of the active site, the chemical environment

around the active site and the binding sites to the support. In other words, control of the catalyst structure and therefore its chemical properties at the atomic scale [1].

The discovery of the M41S family of mesoporous molecular sieves was reported by Beck and coworkers [2, 3]. A great amount of research has been devoted to the well-defined mesoporous molecular sieves that belong to the M41S family. One form of this series, MCM-41 nano-structured materials, which possessed a uniform arrangement of hexagonally shaped mesopores of diameter varying from 20 to 100 Å, has received great attention in materials science and catalysis. The objective is to take advantage of the large pore size of these materials, which will facilitate the flow of reactant and product molecules in and out of the pore system. Large pore systems are needed for shape-selective conversions of bulky molecules such as those increasingly encountered in the refining industry during the upgrading of heavy fractions, oxidation of heavy organics from industrial wastewaters, and in the manufacture of fine chemicals and pharmaceuticals [4–6].

Thus, MCM-41 materials have extended the range of catalytic reaction engineering beyond the micropore domain. Therefore, the exploration of new formulations to generate morphologies and controlled particle sizes of these mesoporous silicates is the crucial step to achieve its extensive applications. In 1997, Unger et al. [7] reported the first synthesis of MCM-41 silicate with spherical morphology in the sub-micrometer size. Later, the same group reported novel pathways controlling the morphology of the product in preparation of MCM-41[8]. They concluded that the addition of alcohol to the reacting mixture led to homogeneous crystallization system favoring the formation of spherical MCM-41 matter. However, the main drawback of these approaches was that the particle size of the obtained products was in sub-micrometer order and the formation of mesostructure usually took long time. Since it is highly desired to apply the MCM-41 type materials to fluidized-bed reactors (FBR) because they can be used to carry out a variety of multiphase catalytic reactions, large-particle mesoporous materials with spherical morphology are demanded [9].

However, pure silica MCM-41 showed limited catalytic applications. Therefore, incorporation of metal centers in the silicate framework is necessary for their use in catalysis. Therefore, isomorphous substitution of silicon with a transition metal is an excellent strategy in creating catalytically active sites and anchoring sites for reactive molecules in the design of new heterogeneous nano-structured catalysts. The incorporation of vanadium, an early member of the 3d transition metal series, in the framework of molecular sieves has resulted in active catalysts for the organic transformations of various substrates using aqueous H_2O_2 as oxidant [10–12].

Particularly, vanadium incorporated molecular sieves have been considered as selective oxidation potential catalysts of large organic molecules under mild conditions [11, 13–17]. The activity and selectivity of these catalysts were found to be sensitive to the nature of V species in the matrix, which includes oxidation state, coordination condition, dispersion, and stability [11, 18]. Besides dispersing and stabilizing vanadium species, structural features of mesoporous supports also have effect on the form of vanadium species and its catalytic behavior. It is noteworthy that a higher concentration of isolated vanadium active sites in the ordered mesoporous lattice can be obtained compared with the conventional silica support [11]. However, coordination, location, and aggregation degree of vanadium in these materials are still not well understood [11, 18–21].

Since in the industrial manufacturing of fine chemicals, the selective oxidation transformations are still widely performed by means of large amounts of organic peroxoacids and of transition metal reagents, the use of V-silicate-based heterogeneous catalysts may contribute remarkably to the set-up of industrial processes environmentally benign. On the other hand, dilute hydrogen peroxide is one of the most convenient oxidants due to its easy handling, high content of active oxygen and absence of byproducts [22]. In this context, the selective oxidation of organic compounds, and especially of the bulky olefinic compounds, employing V-based heterogeneous catalysts and H_2O_2 has gained considerable interest [21, 23].

The aim of this work is to characterize the morphological, structural and surface properties of vanadium-containing mesoporous molecular sieves (V-MMS) MCM-41 type, and correlate structure–activity in the test reaction of oxidation of cyclohexene with H_2O_2. The particle size, morphology and structural regularity of V-MMS have been investigated by electronic microscopy (scanning and transmission), X-ray diffraction and N_2 physisorption. The possible location and distribution of vanadium species in mesoporous silica could be inferred by Ultraviolet–Visible diffuse reflectance measurements. The catalytic properties of the nano-structured materials synthesized were tested for the cyclohexene oxidation reaction with H_2O_2 and the influence of the V loading over active sites efficiency was studied.

2 Experimental

2.1 Catalyst Preparation

The vanadium-containing mesoporous molecular sieves (V-MMS) were prepared using cetyltrimethyl ammonium bromide (CTABr, Aldrich) as template. Tetraethoxysilane (TEOS, Fluka ≥98%) and $VO(SO_4)\cdot H_2O$ (Aldrich,

>99,99%) were used as the Si and V sources, respectively. The pH of the synthesis was adjusted to 13 by adding of a tetraethylammonium hydroxide (TEAOH, Sigma-Aldrich) 20 wt% aqueous solution. The catalysts were synthesized from a gel of molar composition: Si/V = 20, 60 and 240, TEAOH/Si = 0.3, CTABr/Si = 0.3, H_2O/Si = 60. In a typical synthesis, TEOS and $VO(SO_4)\cdot H_2O$ were vigorously mixed for 30 min. Then, 25 wt% solution of CTABr in ethanol and 70% of the TEAOH were added drop wise; this mixture is continuously stirred for 3 h. Finally, the remaining TEAOH and the water were further added drop wise to the milky solution which was then heated at 358 K for 30 min to remove ethanol used in solution and produced in the hydrolysis of TEOS. This gel was treated hydrothermally into a Teflon-lined stainless-steel autoclave and kept in an oven at 373 K for 4 days under autogeneous pressure. The final solids were filtered, washed with distilled water until pH ~7 and dried at 333 K overnight. The colour of the as-synthesized samples was white. The template was evacuated from the samples by heating (2 K/min) under N_2 flow (45 mL/min) at 773 K for 6 h and subsequent calcination at 773 K for 6 h under dry air flow (45 mL/min). The final colour of the calcined samples was white, which turns to pale yellow when the materials are exposed at atmospheric conditions.

2.2 Characterization Techniques

The materials were characterized by powder X-ray diffraction (XRD), nitrogen adsorption/desorption, scanning electronic microscopy (SEM), transmission electronic microscopy (TEM) and Ultraviolet–Visible diffuse reflectance (UV–Vis–DR) spectroscopy. The vanadium content in the final solid products was determined by atomic absorption spectroscopy (AAS) using an AA Varian Spectra spectrophotometer. The samples were previously digested using HF and HNO_3 in a 2:1 ratio, and then were diluted with distilled water until 4.5 mL of solution. The percent relative uncertainty of the AAS results was 5%. XRD patterns were collected in air at room temperature on a PANalytical X'Pert PRO diffractometer using Cu K_α radiation of wavelength 0.15418 nm. Diffraction data were recorded in the 2θ = 1–8°/10–70° ranges at an interval of 0.02° and a scanning speed of 0.7°/min was used. The interplanar distance (d_{100}) was obtained by the Bragg law using the position of the first X-ray diffraction line. The lattice parameter (a_0) of the hexagonal unit cell can be calculated by $a_0 = (2/(3)^{1/2})*d_{100}$. Specific surface area, pore size distribution and total pore volume were determined from N_2 adsorption/desorption isotherms obtained at 77 K using a Micromeritics ASAP 2010 (Accelerated Surface Area and Porosimetry System). The surface area was determined by the Brunauer, Emmett and Teller (BET) method and the pore size distribution by the Barrett, Joyner and Halenda (BJH) method, based on the Kelvin equation and obtained for the adsorption branch [24]. The primary mesoporous volume was estimated by the alpha plot method, the total pore volume by the Gurvischt rule at $P/P_0 \sim 0.98$, and the secondary mesoporous volume by the difference [25]. SEM micrographs were obtained in a JEOL model JSM 6380 LV. Lower resolution TEM images were obtained in a Jeol Model JEM-1200 EXII System. UV–Vis–DR spectra of the materials were recorded under ambient conditions using an Optronics OL 750-427 spectrometer in the wavelength range between 200 and 900 nm. The original spectra obtained for the calcined samples have been fitted in sub-bands using Multi-peaks fit in OriginPro 8 software. Curve-fitting calculations were useful for determining the location of the bands and their areas; the fitting confidence was $\chi^2 \leq 0.0009$ and $R^2 \geq 0.983$.

2.3 Catalytic Activity

The cyclohexene oxidation reactions with H_2O_2 were carried out in a glass reactor with magnetic stirrer, immersed in a thermally controlled bath at 343 K. In a typical reaction, cyclohexene (0.5512 g) was vigorously stirred with H_2O_2 (0.1597 g) using acetonitrile as solvent (4.0700 g) and V-MMS catalyst (0.0054 g). Reaction progress was followed taking samples during reaction through sealed septa by means of a syringe without opening the reactor. Liquid samples were filtered and analyzed by gas chromatography (Hewlett Packard 5890 Serie II) with capillary column (cross-linked methyl-silicone gum—30 m × 0.53 mm × 2.65 mm film thickness) and a FID detector. Reaction products were identified by mass spectrometry (Shimadzu GCMS-QP 5050) with HP-5 capillary column. The total conversion of H_2O_2 was measured by iodometric titration. The cyclohexene conversion was defined as: cyclohexene conversion × 100/theoretically possible conversion (% of max. = Xc). The turnover number (TON) was defined as moles of cyclohexene converted/mol of V. The relative uncertainties of the measurements were tested with repeated determinations. The percent relative uncertainty (CV (%)) of the result was calculated by dividing the corresponding absolute uncertainty with the average of the measurements.

3 Results and Discussion

3.1 Catalyst Characterization

The XRD patterns of the V-MMS catalysts prepared with different vanadium content under hydrothermal treatment

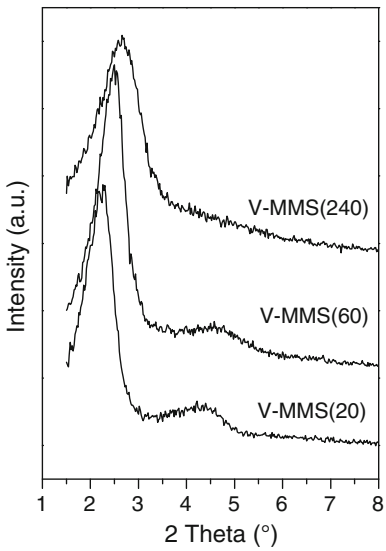

Fig. 1 XRD patterns of the V-MMS catalysts modified with different vanadium content

for 4 days are shown in Fig. 1. As it can be seen, all the samples exhibit a main diffraction peak corresponding to the (100) plane and a weak diffraction peak between 3 and 6° possibly due to the overlapping of the signals of the planes (110) and (200). These signals are characteristic of materials with MCM-41 type mesoporous structure, which remained stable under calcination. Contrary to the explanation given by some authors [26] regarding the loss of structural order that can cause the use of direct synthesis method to introduce metal species in a mesoporous network, all the materials obtained by us showed a well defined structure. Additionally, contrary to the earlier observed results [8, 11, 27] it should be noted that, with the increase in the percentage of vanadium loading, the peak of X-ray intensity of the V-MMS catalysts is increased. This discrepancy can be explained as follows: the simultaneous condensation between metal and silica precursors in the presence of structure directors may enhance the structural ordering, because the metal species act as a promoter for the condensation of the silica species with an increased probability for the incorporation of vanadium into the framework of silica [19, 28].

It is noteworthy that previously this analysis was carried out by XRD measurements (not shown here) to V-MMS materials synthesized at different hydrothermal treatment time (between 0 and 8 days). The best structural regularity was obtained with 4 days of hydrothermal treatment at 373 K, regardless of the vanadium content in the initial synthesis gel. This is possibly due to that a long hydrothermal treatment time at this temperature with a appropriate water content makes easier orient the surfactant-silicate assembly [12]. Additionally, a long time of hydrothermal treatment also promote the incorporation of a greater percentage of vanadium in the silica structure [12].

Although MCM-41 walls are amorphous, if their chemical composition is modified by adding a certain amount of an element different from Si, it is expected that the average unit cell parameter will be affected. This technique is generally accepted as an additionally way of establishing the element location in the silicate framework, or as extra framework species [5, 10, 19, 29, 30]. For our samples, as the content of V is increased (Table 1), the main peak corresponding to plane (100) shifted towards lower diffraction angles and a increase in the parameter a_0, consistent with a probable incorporation of V into the siliceous structure, was observed. Thus, due to the differences in the ionic radius of $V^{\delta+}$ ($V^{4+} = 0.61$ Å and $V^{5+} = 0.59$ Å) and Si^{4+} (0.41 Å), the substitution of the larger $V^{\delta+}$ ion in place of Si^{4+} invariably should distorts the geometry around V from an ideal T_d. Therefore, the length of Si–O–V bond different from that of Si–O–Si, should certainly lead to some structure deformation and consequently contribute to the decrease of surface area.

Finally, it is noteworthy that large angles XRD studies have been performed but no obvious diffraction peaks corresponding to crystalline vanadium oxides can be observed for these samples, suggesting that the vanadium oxide species, if any, are clusters or particles too small to be detected by XRD (crystallites smaller than about 5 nm).

As another method to confirm the highly ordered MCM-41 type structure, the nitrogen physisorption technique (at 77 K) may be used because this type of structure contains a regular pore arrangement so that it presents the typical characteristics of capillary condensation. Therefore if the synthesized sample has a regular pore structure it should show a step increase in the adsorption isotherm due to the capillary condensation at a certain N_2 partial pressure. Figure 2 shows the N_2 adsorption/desorption isotherms (a) with their corresponding BJH pore size distribution (b) of the V-MMS catalysts; the corresponding physical parameters are collected in Table 1. As it can be seen in Fig. 2a, the V-MMS(60) and V-MMS(240) samples exhibit type IV isotherms [31] typical of mesoporous structures, with an inflection at relative pressure $P/P_0 \sim 0.2$–0.4 characteristic of capillary condensation inside the conventional mesopores present in MCM-41 structure (primary or structural mesopores). Such inflection provides a measure of the distribution range of the pore size of these materials [32]. These adsorption isotherms featured a narrow step of capillary condensation, which provides clear evidence of their narrowly defined diameters range for the mesoporous channels of these samples, which is evidenced in Fig. 2b. Additionally, these samples exhibited an increase in the adsorption branch at relative pressures about 0.85, which could be due to a capillary condensation in

Table 1 Structural parameters of the V-MMS synthesized with different V content

Sample	Si/V[a]	$d_{(100)}$ (nm)[b]	a_0 (nm)[c]	D_{BJH} (nm)[d]	t_w (nm)[e]	Mesop. Vol. (cm^3/g, STP)[f]		A_{BET}[g]
						Primary	Secondary	(m^2/g)
V-MMS(20)	20	3.96	4.57	2.65	1.92	0.36	0.04	934
V-MMS(60)	60	3.52	4.06	2.25	1.81	1.03	0.31	1380
V-MMS(240)	240	3.30	3.81	2.45	1.36	1.06	0.45	1370

[a] Molar ratio in the initial synthesis gel; [b] interplanar spacing (100); [c] lattice parameter; [d] BJH pore diameter; [e] wall thickness calculate by $a_0 - D_p$; [f] pore volume; [g] BET specific surface area

secondary mesopores [28–33] or non structural pores [34]. The secondary mesoporous volume for these samples can be seen in Table 1. Moreover, hysteresis loops that resemble H4-type [35] with a sharp decrease in the desorption branch at $P/P_0 \sim 0.45$–0.5, which evidence the existence of ink-bottle pores, can be observed. Additionally, these samples show a parallelism between the adsorption and desorption branches, which is characteristic of slit pores [35]. According to some authors [36, 37], the non-structural porosity is consisting of large cavities eventually interconnected and accessible through necks, which have an average diameter smaller than those of the main voids. Figure 2b, for these samples, also shows broad peak in the distribution of pores size between 20 and 100 nm, which is attributed to this secondary mesoporosity. As it can be observed in Table 1, the V-MMS(60) and V-MMS(240) samples show surface areas $\sim$1300 m^2/g and total pore volumes $\sim$1.35–1.50 cm^3/g, which in turn may help in an easy diffusion of the reactant species to the active metal sites located inside the channel walls. It is noteworthy that the materials synthesized by us have thicker wall than the typical MCM-41 materials ($\sim$0.8 nm) [1], which possibly would confer greater stability to the material under hydrothermal conditions. Moreover, it is possible to observe that the wall thickness increases with the V content. This feature could possibly be due to the presence of metal nano-clusters and/or nano-oxides inside the channels, which would lead to an apparently thicker wall.

On the other hand, the V-MMS(20) sample synthesized with the highest V content shows very different structural characteristics from N_2 physisorption analysis, in contrast with its well defined XRD pattern. This sample exhibits a N_2 adsorption isotherm type I characteristic of microporous materials, which may evidence the existence of microporous domains in this material [38]. As can be seen in Fig. 1a, this catalyst showed a very low adsorption compared with the other ones, which is reflected in the large decrease in the specific surface area as well as in a marked decrease in the number of primary mesopores and in the near disappearance of secondary mesopores (see Table 1). The closure of the hysteresis cycle at pressures relatively $\sim$0.42, accounts for the presence of interconnected pores [36]. The pore distribution in Fig. 2b shows the low amount of pores that possesses this sample as compared to the others, and also show a small increase in its size. Three

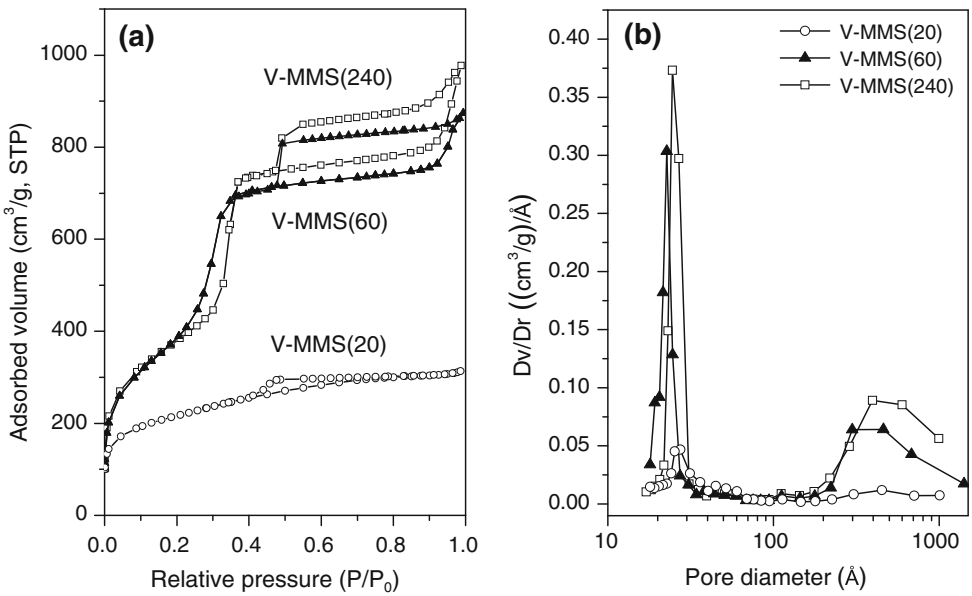

Fig. 2 N_2 adsorption/desorption isotherms (**a**) and BJH pore size distribution (**b**) of the V-MMS catalysts modified with different vanadium content

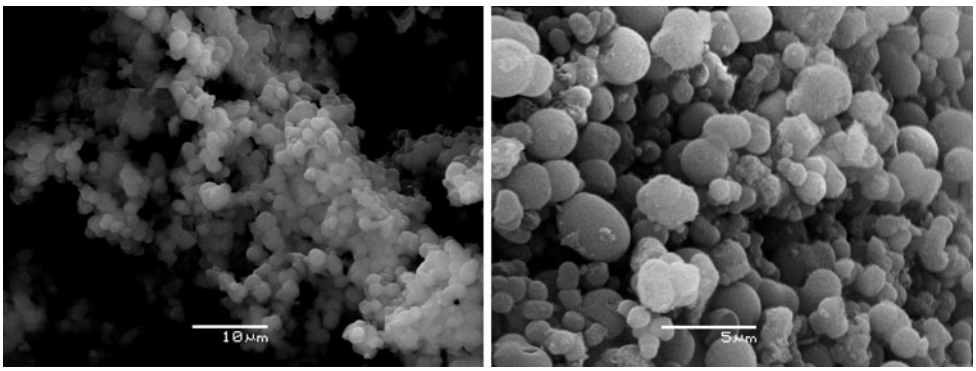

Fig. 3 Scanning electronic microscopy images of V-MMS(20) catalyst

causes could be responsible for these behaviors: the presence of a large number of microporous domains probably due to the formation of V_xO_y nano-oxides; the blocking of the pores caused by such oxides; as well as the deposition of these nano-oxides and/or nano-clusters into the channels causing thicker walls.

The particle size and morphology of V-MMS were investigated by scanning electron microscopy. The formation of various periodic mesoporous materials starts with nucleation, which involves the surfactant–silicate interactions, and these interactions facilitate the assembly of the surfactant–silicate species in the desired morphology [10]. SEM images of the V-MMS(20) sample are showed in Fig. 3, taken as representatives. As it can be seen, these materials show spherical-like morphology in the micrometer-range with a particle-size distribution in the range between 2 and 4 μm. It is noteworthy that exists a substantial amount of fragments in the final V-MMS product, possibly due to time of hydrothermal treatment employed [9]. Nevertheless, these samples exhibit a well-resolved X-ray diffraction pattern. Therefore, it will be expedient to independently optimize the particle morphology and the mesoporous structure characteristic of MCM-41 materials. Pârvalescu et al. [11] also reported spherical morphology for samples V-MCM-41 prepared by hydrothermal synthesis during 5 days but the particle-diameter distribution reported was between 0.2 and 1.2 μm. On the other hand, Jha et al. [10] reported that the presence of foreign ions in the synthesis gel alters the structure directing action of the template and the attenuations further depend on the nature of metal source used. However, images of V-MMS and Cu-MMS [39] nanostructured materials prepared by us through direct incorporation methods, reveal that the spherical morphology (between 2 and 4 μm) of our materials is independent of both the type of metallic cation employed as well as the metal content in the initial synthesis gel.

Transmission electron microscopy studies of the V-MMS materials were made in order to examine their structural regularity. Figure 4 (a) and (b) shows TEM images of sample V-MMS(20) sample, taken as representatives of these materials. Additionally, (c) and (d) images were also taken in the V-MMS(60) and V-MMS(240) samples, respectively. As it is seen, these materials present a well-defined mesoporous structure. However, these micrographs do not show the typical hexagonal pore arrangement of MCM-41 type materials. On the other hand, as it can be observed in the (c) and (d) micrographs, regions of low contrast randomly interrupt the pores arrangement characteristic of the mesoporous material. Such weak regions can be attributed to the presence of cavities that permeate the entire bulk, giving rise to the secondary porosity mentioned above [30, 33]. A the genesis of the secondary mesopores is not fully understood, Díaz et al. [33] have reported that a change in the micellar size might favor the change from cylindrical micelles to more complex aggregates. These aggregates would be responsible for the building-up of such secondary porosity. A great amount of V in the synthesis medium may interfere in the formation of the micelles by changing its ionic strength, giving rise to these complex aggregates. It is noteworthy that unlike the images of Cu-MMS materials [39], recently reported by us, these V-MMS catalysts do not show high-contrast that interrupt the pores arrangement, which in TEM images are attributed to oxide particles segregated from structure. The vanadium-species have not been detected in these TEM micrographs probably due to very little small size and/or also at the low resolution of the measuring equipment.

The UV–Vis–DR spectra were recorded to understand the coordination environment of V species in the MCM-41 type structure. This technique is useful and reliable in the detection of the presence of framework and extra-framework metal species in metal-containing mesoporous materials. It is known that the metal species in framework positions are the active sites for carrying out selective catalytic oxidations of hydrocarbons using peroxides as oxidants [5, 11, 12, 40]. Moreover, nano-oxides crystallites segregated of the mesoporous silicates were proved to lower the catalytic performance by enhancing the decomposition of H_2O_2 into water and oxygen [40]. Therefore, it becomes very crucial to control the synthesis parameters in order to obtain oxides-free mesoporous silicates maximizing the presence of isolated framework metal species [37, 41].

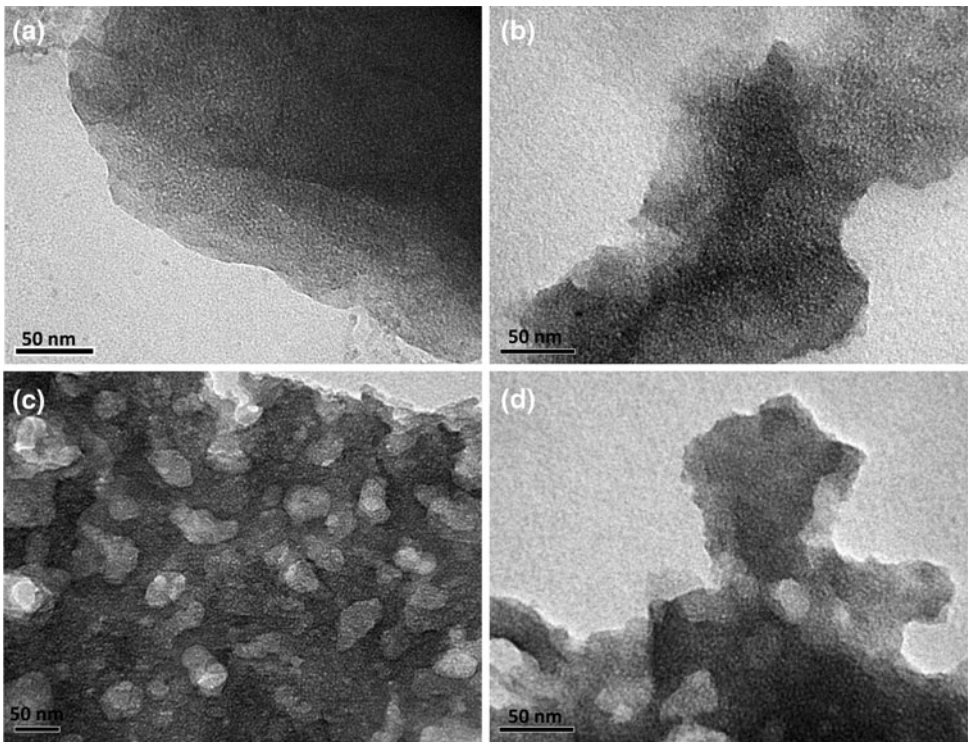

Fig. 4 Transmission electronic microscopy images of V-MMS catalysts. **a**, **b** correspond to V-MMS(20); **c**, **d** correspond to V-MMS(60) and V-MMS(240), respectively

The UV–Vis–DR spectra for the calcined V-MMS catalysts recorded under ambient conditions are shown in Fig. 5. The Si/V atomic ratio and the overall metal content in the final solid as well as the distribution of vanadium species, determined by UV–Vis–DR, are presented in Table 2. The original spectra have been deconvoluted into sub-bands to facilitate the assignment to the different V species.

The intense ligand-to-metal charge transfer band around ~260 nm present in all our samples clearly indicates that most of V ions are isolated and in tetrahedral (T_d) coordination possibly with the lattice oxygen [5, 21, 37, 38, 42].

The second band ~370 nm becomes significant in the samples with relatively high V content indicating the presence of higher coordinated V ions (penta-, or hexacoordinated) co-existing to a small extent with the tetrahedral V sites. This higher coordination environment of V cations could also appear upon hydration by insertion of water molecules as extraligands to the V T_d species during preparation [10, 12, 20, 38]. Both the highly hydrophilic surface and the high surface area of these materials yield a high water adsorption capacity which would lead to a high hydration of surface V ions. However, the possibility of some $(V–O–V)_n$ clustering in the framework due to an incipient oligomerization of V species containing $(V–O–V)_n$ bonds cannot be unequivocally excluded [5, 20, 38]. At this respect, Peña et al. [20] reported UV–Vis–DR measurements of dehydrated V-MCM-41 materials prepared by impregnation method. They concluded that for materials with low V content (<0.5 wt%) the band around ~370 nm disappears when are dehydrated at a temperature above 673 K. While that for materials with high V loading (>0.8 wt%) a shoulder around 370 nm is still observed which is associated to polymeric $(V–O–V)_n$ clusters species.

It is noteworthy that for the V-MMS(240) catalyst, the band around ~370 nm is not prominent, and this suggests that at lower vanadium contents non-accessible tetrahedral vanadium sites may be the possible type of local environment present, where the water molecules cannot access the V sites to increase the coordination. Moreover some authors observed that the band absorption at the 260 nm is not influenced by moisture treatments, whereas the bands above 360 nm are modified by various treatments [12, 43]. This anomalous behavior could be interpreted for the presence of two different kinds of V species on the samples, one well buried inside the pore channels, which are thermally and chemically stable, and the other on the hexagonal wall surfaces, which can easily undergo modifications [12].

Finally, a new band around ~450 nm only appears for the V-MMS(20) catalyst. This band could be attributed to V ions in the octahedral symmetry in V_xO_y crystallites.[18–21, 38] These nano-oxides can possibly be generated as consequence of a further polymerization degree of the V species due to the highest of V content in the initial synthesis gel [18, 21, 38]. Thus, the UV–Vis–DR analysis allows us to suggest the presence of vanadium nano-oxide even as the same could not be detected by XRD.

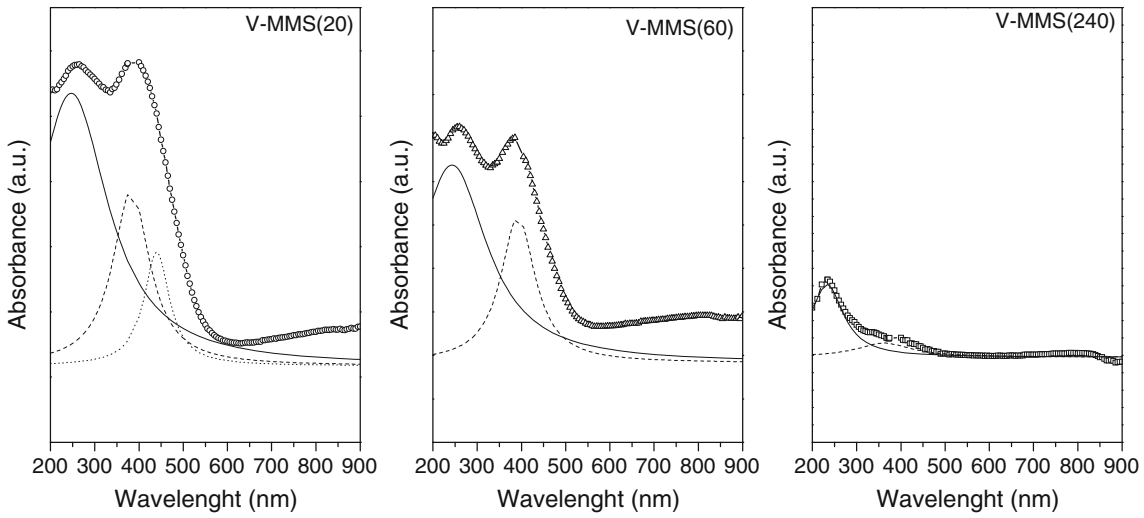

Fig. 5 UV–Vis diffuse reflectance spectra of the calcined V-MMS catalysts recorded under ambient conditions. Deconvoluted sub-bands: *solid line* isolated $V^{\delta+}$, *dashed line* $[V^{\delta+}\cdots O^{\delta-}\cdots V^{\delta+}]_n$ nano-clusters, *dotted line* V_2O_5 nano-oxides

Table 2 Chemical composition and vanadium species relative distribution in V-MMS modified with different vanadium content

Sample	V content [wt.%][a]	Si/V[a]	Distribution of vanadium species					
			Isolated ions		Clusters and/or hydrated ions		Oxides	
			% area	% V	% area	% V	% area	% V
V-MMS(20)	1.210	71.5	0.68	0.823	0.22	0.266	0.10	0.121
V-MMS(60)	0.140	676.8	0.73	0.102	0.27	0.038	0.00	0.00
V-MMS(240)	0.035	2416.3	0.75	0.026	0.25	0.009	0.00	0.00

[a] In the final solid

Table 2 shows an estimation of the percentage of the different V species in the samples. Distribution of these V species depends on the quantity of vanadium in the initial gel. Judging by the relative percentage of sub-bands area, the isolated V ions seems to play a dominant role in the case of the samples prepared with the lower V content. Meanwhile, the increase of V content would probably increase the degree of polymerization of the V species. Furthermore, it is notable that only the V-MMS(20) sample evidenced the existence of V_xO_y nano-oxides. In this table, it is also shown a marked increase in the Si/V molar ratio of the final solids with respect to the same ratio in the initial synthesis gel. This possibly indicates that only a small proportion of the vanadium initially introduced into the synthesis gel is retained by the siliceous structure.

3.2 Catalytic Activity

The catalysts synthesized with different V contents were evaluated in the reaction of cyclohexene oxidation with H_2O_2 at 343 K; their catalytic activities are shown in Fig. 6. As it can be seen, when the vanadium content increased from 0.035 to 0.140 wt.% the conversion of cyclohexene presented a marked increase (~93%), whereas the V-MMS(20) sample modified with higher content showed the lowest activity. These results could be interpreted taking into account the higher proportion of V ions isolated in a distorted tetrahedral coordination present in the samples V-MMS(60) and V-MMS(240) which would be possibly the active catalytic species in this reaction. Moreover, the H_2O_2 conversion increases with the V content in the samples, while its efficiency shows an opposite trend (see Table 3). This behavior could be attributed to the fact that the material with higher V loading presents higher proportion of clusters species and/or V_xO_y nano-oxides observed by UV–Vis–DR measurements. These species would be responsible for the decomposition of peroxide to water, resulting in a lower cyclohexene conversion. Besides, according to the XRD analyses and the N_2 adsorption/desorption isotherms, this material presents a smaller surface area and pores volume than those with lower vanadium content. Probably, V_xO_y nano-particles might be placed inside the material channels, as well as on the external surface, thus diminishing or blocking the accessibility to the active sites (isolated V ions), what cause a decrease of the catalytic activity.

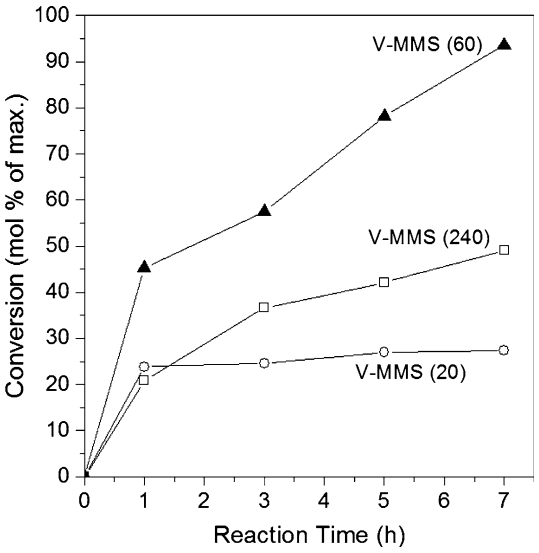

Fig. 6 Catalytic activities in oxidation of cyclohexene with H_2O_2 over V-MMS catalysts. Reactions conditions: cyclohexene/H_2O_2 (mol/mol) = 4/1, temperature = 343 K

Scheme 1 shows the different products observed and the results of selectivity are presented in Table 3. GC–MS analyses indicated that the products mixture was mainly composed of products resulting from both the oxidation of C=C double bond (cyclohexene oxide and 1,2 cyclohexanodiol) and allylic C–H bonds (2-cyclohexen-1-ol and 2-cyclohexen-1-one) (Table 2). In practice, epoxidation and allylic oxidation are often competitive processes in the oxidation of cyclic olefins and frequently both processes occur simultaneously giving a mixture of reaction products. As it can be observed, the selectivity to epoxide decreases with the increase of the vanadium loading, increasing simultaneously the selectivity to 1,2 cyclohexanodiol as the result of the opening of the epoxide. With regard to the allylic products, the selectivity to 2-cyclohexen-1-ol remains almost constant whereas the values for 2-cyclohexen-1-one decrease with the metal increase. Besides, the appearance of 2,3 epoxi-cyclohexenone was observed. According to these results, the last product (V) would probably result from the epoxidation of the double bond of the 2-cyclohexen-1-one.

Furthermore, the turnover numbers (TON) are also given in Table 3. They decrease markedly with increasing metal content which would confirm that, as it was discussed above, much of vanadium is not effectively used during the catalytic oxidation. Therefore, the high activity and efficiency presented by the material with lower metal loading would be giving account for the high dispersion of the active sites obtained on this material.

Farzaneh et al. [44] reported a cyclohexene conversion with TBHP and V-MCM-41 (olefin/oxidant molar ratio = 20/24) around 27% using $CHCl_3$ as solvent and around 8% with acetonitrile, which is much lower compared to our results (24.5%; 92,5% of max.), using both eco-compatible oxidant and solvent and an excess of olefin.

4 Conclusions

Mesoporous silicate particles with spherical morphology containing nano-sized vanadium species were synthesized by conventional hydrothermal synthesis. The V-MMS catalysts showed a narrow particle-size distribution in the range between 2 and 4 μm. TEM images of these materials showed a well-defined mesoporous structure. However, these micrographs not showed the typical hexagonal pore arrangement of MCM-41 type materials. Additionally, secondary mesoporosity domains were determined in the BJH size distribution. All the materials exhibited a good structural regularity besides specific surface areas above 900 m^2/g and pore volume of about 1 cm^3/g, which are

Table 3 Cyclohexene oxidation with H_2O_2 and V-MMS catalysts

Sample	Time (h)	TON[a]	H_2O_2 conversion (mol%)[b]	H_2O_2 efficiency (mol %)[c]	Selectivity (mol %)[d]				
					(I)	(II)	(III)	(IV)	(V)
V-MMS (20)	1	42.12	95.80	24.84	1.92	27.94	29.36	18.70	22.07
	7	48.41	100.00	27.40	0.00	30.52	27.23	17.60	24.65
V-MMS (60)	1	546.93	70.27	64.39	8.56	28.75	25.09	24.34	13.26
	7	1087.34	95.39	96.44	7.79	24.21	26.02	26.82	15.16
V-MMS (240)	1	905.03	25.73	80.92	9.92	25.39	24.43	40.26	0.00
	7	2131.41	48.98	100	7.70	24.66	26.81	40.83	0.00

[a] *TON* moles of cyclohexene converted/mol of vanadium. CV <7%

[b] CV <5%

[c] H_2O_2 efficiency = moles of products formed(I–V)/mol of H_2O_2 reacted. CV <7%

[d] Selectivity = (mol product/mol total products) × 100. CV <5%. (I): cyclohexene oxide, (II): 1,2-cyclohexanediol, (III): 2-cyclohexen-1-ol, (IV): 2-cyclohexen-1-one, (V): 2,3- epoxy-cyclohexanone

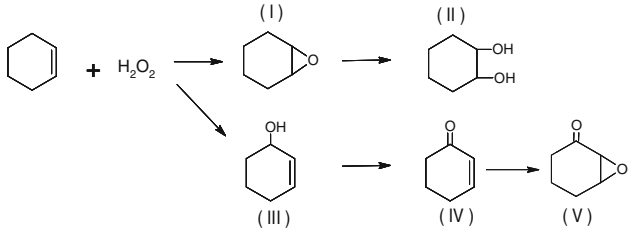

Scheme 1 Products obtained from cyclohexene oxidation. Epoxidation: cyclohexene oxide (I) and 1–2 cyclohexanediol (II); allylic oxidation: 2-cyclohexen-1-ol (III), 2-cyclohexen-1-one (IV) and 2,3-epoxy-cyclohexanone (V)

typical of these mesoporous materials. However, the sample synthesized with the highest content of V $\sim$1.21 wt% presented marked differences in their structural characteristics, which was attributed to the presence of like nanoclusters and/or V_xO_y nano-oxides extra-framework species. A successful incorporation of isolated V cations to silica structure in tetrahedral coordination with oxygen of the network can be inferred from UV–Vis–DR analysis. The catalytic activity of V-MMS was evaluated in the test reaction of cyclohexene oxidation using H_2O_2 as an oxidant agent. These catalysts showed a very good conversion of cyclohexene, $\sim$93% of maximum, and a high selectivity towards allylic oxidation products. Probably the isolated V ions, incorporated into the silica structure, would be responsible for the high catalytic activity of these materials. Therefore, from the obtained results of this catalytic test, we can conclude that V-MMS are potential catalysts for the bulky olefins oxidation.

Acknowledgment G.A.E., K.S. and S.G.C are CONICET Researchers; C.M.Ch. and A.L.C received CONICET Doctoral Fellowship. This work was supported by the CONICET, the UTN-FRC and the UNSL of Argentina, and UdeC of Chile. We thank J. Bazán Aguirre (UTN-FRC Student) for valuable help on some experimental activities. Finally, C.M.Ch. acknowledge to Dra. M.E. Crivello for the participation in international cooperation project MINCYT–CONICYT, Code CH/08/03.

References

1. Soller-Illia GJAA, Sanchez C, Lebeau B, Patarin J (2002) Chem Rev 4093:102
2. Kresge CT, Leonowicz ME, Roth WJ, Vartuli JC, Beck JS (1992) Nature 359:710
3. Beck JS, Vartuli JC, Roth WJ, Leonowicz ME, Kresge CT, Schmitt KD, Chu CT-W, Olson DH, Sheppard EW, McCullen SB, Higgins JB, Schlenker JL (1992) J Am Chem Soc 114:10834
4. Reddy EP, Davydov L, Smirniotis PG (2002) J Phys Chem B 106:3394
5. Eimer GA, Casuscelli SG, Ghione GE, Crivello ME, Herrero ER (2006) Appl Catal A 298:232
6. Eimer GA, Casuscelli SG, Chanquía CM, Elías V, Crivello ME, Herrero ER (2008) Catal Today 133–135:639
7. Grün M, Lauer I, Unger KK (1997) Adv Mater 9:254
8. Szegedi Á, Kónya Z, Méhn D, Solymár E, Pál-Borbély G, Horváth ZE, Biró LP, Kiricsi I (2004) Appl Catal A 272:257
9. Liu X, Sun H, Chen Y, Yang Y, Borgna A (2009) Microporous Mesoporous Mater 121:73
10. Jha RK, Shylesh S, Bhoware SS, Singh AP (2006) Microporous Mesoporous Mater 95:154
11. Pârvulescu V, Anastasescu C, Su BL (2003) J Mol Catal A 198:249
12. Shylesh S, Singh AP (2005) J Catal 233:359
13. Reddy KM, Moudrakovski I, Sayari A (1994) J Chem Soc Chem Commun 1059
14. Gontier S, Tuel A (1995) Microporous Mater 5:161
15. Morey M, Davidson A, Eckert H, Stucky G (1996) Chem Mater 8:486
16. Moudrakovski I, Sayari A, Ratcliffe CI, Ripmeester JA, Preston KF (1994) J Phys Chem 98:10895
17. Pârvulescu V, Su BL (2001) Catal Today 69:315
18. Chao KJ, Wu CN, Chang H, Lee LJ, Hu S-f (1997) J Phys Chem B 101:6341
19. George J, Shylesh S, Singh AP (2005) Appl Catal A 290:148
20. Peña ML, Dejoz A, Fornés V, Rey F, Vázquez MI, López Nieto JM (2001) Appl Catal A 209:155
21. Gao F, Zhang Y, Wan H, Kon Y, Wu X, Dong L, Li B, Chen Y (2008) Microporous Mesoporous Mater 110:508
22. Sanderson W (2000) Pure Appl Chem 72:1289
23. Weckhuysen BM, Keller DE (2003) Catal Today 78:25
24. Gregg SJ, Sing KSW (1982) Adsorption, surface area and porosity. Academic Press, New York
25. Sayari A, Liu P, Kruk M, Jaroniec M (1997) Chem Mater 9:2499
26. Hao X-Y, Zhang Y-Q, Wang J-W, Zhou W, Zhang C, Liu S (2005) Microporous Mesoporous Mater 88:38
27. Velu S, Wang L, Okazaki M, Suzuki K, Tomura S (2002) Microporous Mesoporous Mater 54:113
28. Parvulescu V, Anastasescu C, Su BL (2003) J Mol Catal A Chem 3919:1
29. Gomes HT, Selvam P, Dapurkar SE, Figueiredo JL, Faria JL (2005) Microporous Mesoporous Mater 86:287
30. Eimer GA, Chanquía CM, Sapag K, Herrero ER (2008) Microporous Mesoporous Mater 116:670
31. Sing KSW, Everett DH, Haul RAW, Moscou Pierotti L, Rouquerol RA, Siemieniewska J (1985) Pure Appl Chem 57:603
32. Kruk M, Jaroniec M, Ryoo R, Kim JM (1999) Chem Mater 11: 2568
33. Díaz I, Pérez-Pariente J (2002) Chem Mater 14:4641
34. Lim S, Haller GL (2002) J Phys Chem B 106:8437
35. Rouquerol F, Rouquerol J, Sing K (1999) Adsorption by powders and porous solids. Principles, methodology and application. Academic Press, London
36. Efremov D, Fenelonov V (1991) Stud Surf Sci Catal 62:62
37. Chanquía CM, Sapag K, Rodríguez-Castellón E, Herrero ER, Eimer GA (2010) J Phys Chem C 114:1481
38. Solsona B, Blasco T, López JM, Peña ML, Rey F, Vidal-Moya A (2001) J Catal 203:443
39. Chanquía CM, Andrini L, Fernández JD, Crivello ME, Requejo FG, Herrero ER, Eimer GA (2010) J Phys Chem C 114:12221
40. Eimer GA, Díaz I, Sastre E, Casuscelli SG, Crivello ME, Herrero ER, Perez-Pariente J (2008) Appl Catal A 343:77
41. Notari B (1996) Adv Catal 41:253
42. Hu Y, Higashimoto S, Takahashi S, Nagai Y, Anpo M (2005) Catal Lett 100:35
43. Luan Z, Xu J, He H, Klinowski J, Kevan L (1996) J Phys Chem 100:19595
44. Farzaneh F, Zamanifar E, Williams CD (2004) J Mol Catal A 218:203